Finite Elements Used in the Vertical Discretization of the Fully Compressible Core of the ALADIN System

JOZEF VIVODA

Slovak Hydrometeorological Institute, Bratislava, Slovakia

PETRA SMOLÍKOVÁ

Czech Hydrometeorological Institute, Prague, Czech Republic

JUAN SIMARRO

Agencia Estatal de Meteorología, Valencia, Spain

(Manuscript received 13 February 2018, in final form 22 May 2018)

ABSTRACT

The finite-element method with B splines is used for definition of vertical operators in the nonhydrostatic fully compressible dynamical core of the ALADIN system. It represents a generalization of the same method used in the hydrostatic dynamical core shared by the ALADIN system and the global forecast system ARPEGE/IFS. The method is shown to be robust enough in idealized academic tests and real simulations. Its theoretical superiority is shown when compared with the finite-difference method.

1. Introduction

The nonhydrostatic effects start to play a significant role when the dimension of both the horizontal and vertical scales of motion become comparable. This happens typically when reaching a horizontal grid size of around 2 km. Aimed at achieving those scales, nonhydrostatic dynamics was introduced in the originally hydrostatic limited-area NWP system ALADIN. The fully compressible nonhydrostatic dynamical kernel of the ALADIN system was designed following the rule that it keeps as many features of its hydrostatic version as possible. The basic choices made are as follows: the spectral technique used for the horizontal spatial discretization, semi-implicit time stepping, and semi-Lagrangian advection [see Bubnová et al. (1995) and Bénard et al. (2010) for details].

For vertical discretization, the finite-difference (FD) scheme of Simmons and Burridge (1981) was applied since the beginning of the project, innovated with the semi-Lagrangian vertical advection according to Ritchie et al. (1995). This scheme is only first-order accurate for nonuniform spacing of vertical levels. An alternative finite-element (FE) vertical discretization was implemented in the hydrostatic core of the ALADIN system and in the global forecast system ARPEGE/IFS by Untch and Hortal (2004). A remarkable fact is that, with the hydrostatic approximation and the semi-Lagrangian advection, the only vertical operations needed are vertical integrals. Therefore, an integral operator was derived based on the Galerkin method using cubic B splines with compact support as basis functions. Also, the use of piecewise linear B-spline basis functions was implemented as an alternative option. It was shown that the FE scheme gives more accurate phase speeds of most of the linear gravity waves than the FD scheme. In addition, the cubic FE scheme has proven to be eighth-order accurate for integrating smooth functions, compared to the first-order accuracy of the FD method. Furthermore, the FE scheme reduces the level of vertical noise in forecasts with the full hydrostatic model of ECMWF, reduces the cold bias in the lower atmosphere, and improves the transport in the stratosphere. Consecutively, the FE vertical discretization has been tested in several hydrostatic

Corresponding author: Petra Smolíková, petra.smolikova@chmi.cz

DOI: 10.1175/MWR-D-18-0043.1

applications of the limited-area model ALADIN, with detected positive impact on the objective verification scores. On top of that, the FE method has proven beneficial in 2D vertical plane idealized tests of a resting, hydrostatically balanced state. Finally, but not less important, the computational cost of such an improvement in accuracy is negligible, because the FE integral operator is defined once in the setup of the model, and it is used in the model, otherwise, exactly in the same way as the FD integral operator.

Not surprisingly, a need has emerged to extend the FE method to the vertical discretization of the fully compressible dynamical core of the ALADIN system. This task has shown to be more intricate and troublesome. Contrary to the hydrostatic equations in a mass-based vertical coordinate, where only the vertical integral operator appears, and to the fully compressible system of equations cast in a height-based coordinate, where only the vertical derivative operator occurs (Simarro and Hortal 2012), in the fully compressible Euler equations of the ALADIN system designed for the mass-based vertical coordinate, both the integral and the derivative vertical operators appear (Laprise 1992).

The difficulty lies not in the necessity to define both sets of operators, but in the need to define them consistently in order to assure the stability and accuracy of the model. There are two points in the nonhydrostatic dynamical core of the ALADIN system where the replacement of the FD operators by the high-order FE operators must be done carefully.

The first crucial point is the semi-implicit scheme. As it is explained in Bubnová et al. (1995), in the semi-implicit step of the ALADIN system, an implicit linear system is solved separately for each horizontal spectral eigenfunction. The unknowns are here the amplitudes of the prognostic variables at each model level for the next time step. The procedure is to reduce the system to a Helmholtz equation for the vertical divergence amplitudes. Because of this reduction, and for stability reasons, an analytic relation involving vertical operators, the so-called C1 constraint, must be fulfilled by the discrete version of those operators (see section 5b and appendix B for C1 definition). The FD operators of the nonhydrostatic dynamical core of the ALADIN system are defined in such a way that C1 constraint is satisfied. However, if the vertical operators do not fulfill the C1 constraint, as it is the case for the FE operators defined in this work, an alternative method must be adopted. We stop the reduction of the implicit linear system toward the Helmholtz equation just before the point where the C1 constraint is used. In this way, a linear system involving the vertical divergence and horizontal divergence amplitudes appears, which is solved iteratively. Such a solution converges in all tested idealized and real cases and, because of the choice of a convenient preconditioning of the system, one iteration of the implicit solver is enough to reach satisfying results. The computational price to be paid is very small and does not penalize the whole integration significantly.

The second crucial point is the transformation between the vertical divergence, used in the spectral calculations for stability reasons explained in Bénard et al. (2004, 2005), and the vertical velocity, used in the grid-point calculations. This transformation must be invertible, and it implies that integral and derivative vertical operators cannot be defined independently. This goal is not fulfilled for FE operators up to now, and the transformations between the vertical divergence and the vertical velocity are still FD ones. The accuracy reached in real forecasts may thus be limited by this fact, and it is foreseen to include invertible high-order transformations between vertical velocity and vertical divergence in the future.

In this paper we follow the notation of the reference papers Bubnová et al. (1995) and Bénard et al. (2010), with small differences. Functions that appear in the paper are mostly space and time dependent. We omit the horizontal space and the time dependence, since we are interested in the vertical space dependence only. Continuous functions are written in lightface italic font (f), discrete functions represented as vectors of values at individual vertical levels are written in boldface roman font ($\mathbf{f}$), analytic linear operators are written in calligraphic font ($\mathscr{P}$), and discrete operators represented as matrices are written in underlined, boldface sans serif font ($\underline{\mathbf{P}}$). Moreover, a vector $\mathbf{f}$ contains values in the physical space, while $\hat{\mathbf{f}}$ contains values in the B-spline function basis space. For the latter one, a basis of B-spline functions must be specified.

The paper is organized as follows. In section 2, model variables and the set of equations used are presented. In section 3, the definition of discrete vertical operators based on FE is described, while vertical operator accuracy is discussed in section 4. A semi-implicit time scheme and the consequences that the usage of FE method in vertical has on its design are given in section 5. Results of idealized test cases are shown in section 6, where the comparison with reference cases using the FD method is shown. Real case experiments are presented in section 7 with the average computational time needed for their execution. Section 8 summarizes the results achieved, outlines future directions, and concludes the paper.

2. Model variables and equations

The aim of this work is to develop a set of high-resolution FE vertical operators and to implement it in the nonhydrostatic fully compressible dynamical core of the ALADIN system. Therefore, the model equations are exactly the same as those detailed in Bénard et al. (2010). For completeness, we rewrite the model equations here, with some simplifications in order to make the reading easier.

For the sake of simplicity we restrict ourselves to the dry shallow atmosphere and omit the Coriolis, frictional, and diabatic forcing. On top of prognostic variables used in the hydrostatic core of the ALADIN system, which are the horizontal velocity vector V with two components, temperature T, and logarithm of hydrostatic surface pressure $q_s = \ln(\pi_s)$, there are two additional nonhydrostatic variables in the fully compressible core of the ALADIN system: a measure of the pressure departure from the hydrostatic value,

$$\hat{q} = \ln\frac{p}{\pi}, \tag{1}$$

and vertical velocity w. Here p is the true pressure, and π is hydrostatic pressure calculated as $\pi = A(\eta) + B(\eta)\pi_s$, where $A(\eta)$ and $B(\eta)$ are horizontally constant chosen functions that implicitly define the vertical coordinate η (Simmons and Burridge 1981). The fully compressible Euler equations of the ALADIN system in the hybrid-mass-based vertical coordinate η for the set of prognostic variables $(V, w, T, \hat{q}, q_s)$ are written as follows:

$$\frac{dV}{dt} = -\frac{RT}{p}\nabla p - \left(\frac{p}{\pi} + \frac{p}{m}\frac{\partial\hat{q}}{\partial\eta}\right)\nabla\phi, \tag{2}$$

$$\frac{dw}{dt} = \frac{g}{m}\frac{\partial(p-\pi)}{\partial\eta}, \tag{3}$$

$$\frac{dT}{dt} = -\frac{RT}{C_v}D_3, \tag{4}$$

$$\frac{d\hat{q}}{dt} = -\frac{C_p}{C_v}D_3 - \frac{\omega}{\pi}, \tag{5}$$

$$\frac{\partial q_s}{\partial t} = -\frac{1}{\pi_s}\int_0^1 \nabla\cdot(mV)\,d\eta, \tag{6}$$

where ∇ is the gradient along the constant η surfaces; R is the perfect gas constant for dry air; g is the acceleration of gravity; $m = \partial\pi/\partial\eta$ is the vertical metric factor; ϕ is the geopotential; C_p and C_v are the specific heat capacities of dry air at constant pressure and volume, respectively; ω indicates the mass-based vertical velocity diagnosed from

$$\omega = \frac{d\pi}{dt} = V\cdot\nabla\pi - \int_0^\eta \nabla\cdot(mV)\,d\eta; \tag{7}$$

and D_3 stands for the local tridimensional divergence:

$$D_3 = \nabla\cdot V - g\frac{p}{mRT}\frac{\partial w}{\partial\eta} + \frac{p}{mRT}\nabla\phi\cdot\frac{\partial V}{\partial\eta}. \tag{8}$$

The geopotential ϕ is obtained through an upward integration of atmospheric depths from the surface geopotential ϕ_s using

$$\phi = \phi_s + \int_\eta^1 \frac{mRT}{p}\,d\eta. \tag{9}$$

The total derivative operator on the left-hand sides of the prognostic equations is defined as

$$\frac{d}{dt} \equiv \frac{\partial}{\partial t} + V\cdot\nabla + \dot{\eta}\frac{\partial}{\partial\eta}. \tag{10}$$

Finally, to complete the system a diagnostic relation for the vertical velocity at the surface yields

$$w_s = \frac{1}{g}V_s\cdot\nabla\phi_s, \tag{11}$$

and the total time derivative of the vertical coordinate is given by

$$\dot{\eta} = B(\eta)\frac{1}{m}\int_0^1 \nabla\cdot(mV)\,d\eta - \frac{1}{m}\int_0^\eta \nabla\cdot(mV)\,d\eta. \tag{12}$$

3. Finite-element scheme

To solve numerically the equations briefly described in the previous section, the spatial domain is discretized horizontally and vertically. In the vertical, the model domain is divided into a number of L layers, using the mass-based vertical coordinate described in Simmons and Burridge (1981). The full model levels are located inside these layers, while the half model levels are located at the material boundaries, that is, at the top and bottom of the atmosphere, and at the interfaces between layers. The model variables are staggered in the vertical direction, being all the variables defined at full levels, with the exception of the vertical velocity, which is located at half levels. See Fig. 1 for vertical staggering illustration.

On the other hand, the horizontal discretization is spectral based on the use of eigenfunctions of the horizontal Laplacian operator, and all horizontal derivatives are calculated in the spectral space

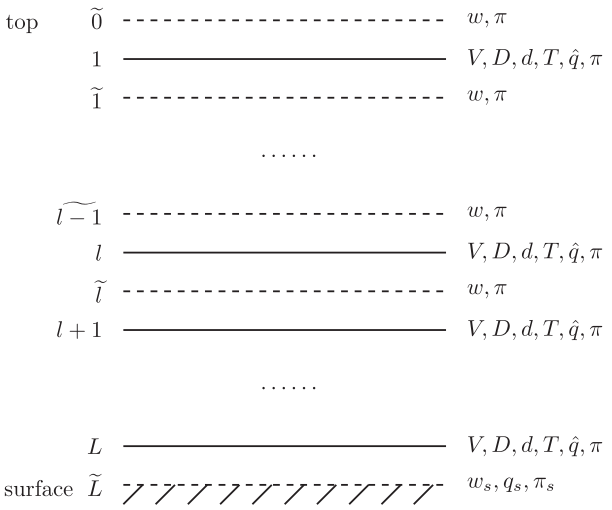

FIG. 1. Staggering of variables among vertical half and full model levels.

(Bubnová et al. 1995). In the following, we omit the horizontal direction, as this work is focused on vertical operators.

The method used for constructing FE operators is similar to the procedure described in Untch and Hortal (2004). However, there are differences, mainly, as it is explained later in this section, the inclusion of boundary conditions that are applied to the input and output functions and the general order of basis functions used. To make a clearer exposition of the method, we first describe how the vertical operators are used in the model.

Let us consider an unknown continuous function $f(\eta)$ as an input, from which just a discrete representation $\mathbf{f}$ is known, which consists of the values of the function f at the L full model levels:

$$\mathbf{f} = (f_1, \ldots, f_L)^{\mathrm{T}} = [f(\eta_1), \ldots, f(\eta_L)]^{\mathrm{T}}. \tag{13}$$

For a linear operator $\mathscr{P}$, defined analytically, we want to find a high-order discrete representation. That is, a matrix $\underline{\mathbf{P}}$ such that

$$\underline{\mathbf{P}} \cdot \mathbf{f} \approx \left[\mathscr{P}(f)(\eta'_1), \ldots, \mathscr{P}(f)\left(\eta'_{L'}\right)\right]^{\mathrm{T}}. \tag{14}$$

The output levels $\eta'_1, \ldots, \eta'_{L'}$ are not necessarily equal to the input levels $\eta_1, \ldots, \eta_L$, although it will be the case for all the operators we define, except one (viz., $\underline{\mathbf{D}_h}$ in Table 1).

Now, we introduce a novelty with respect to the method described in Untch and Hortal (2004). The discrete representation $\underline{\mathbf{P}}$ of a linear operator $\mathscr{P}$ may force the input function $f(\eta)$ to satisfy some linear boundary conditions. For example, discrete representation of the input function can be forced to be zero at the top of the atmosphere, $f(0) = 0$, or to have zero derivative at the surface, $f'(1) = 0$. Similarly, the output function $g(\eta) = \mathscr{P}(f)(\eta)$ discrete representation may be forced to satisfy some linear boundary conditions. In some cases, the boundary conditions are analytical properties of the operators being discretized. In other cases, we found out that the boundary conditions are crucial to achieve stability in the semi-implicit scheme, although, we did not find the way to mathematically demonstrate this fact. In any case, the conditions imposed on the input and output functions being derived from model variables are fully compatible with physical properties of these variables. The complete list of used operators is in Table 1 with linear boundary conditions specified. Notice that there are four versions of the first derivative operator, each of them is used at different positions of the linear and nonlinear model equations, as is shown later; $\underline{\mathbf{D}_q}$ and $\underline{\mathbf{D}_h}$ share the same boundary conditions, but they differ in used output vertical levels as described later.

TABLE 1. Boundary conditions for discrete FE operators used in the model. Input and output functions are $f(\eta)$ and $g(\eta)$, respectively.

Operator	Analytic representation	Top BC	Bottom BC
$\underline{\mathbf{D}_p}$	$\frac{\partial}{\partial \eta}$	$f(0) = 0$ $f'(0) = 0$	$f(1) = 0$ $f'(1) = 0$
$\underline{\mathbf{D}_q}$, $\underline{\mathbf{D}_h}$	$\frac{\partial}{\partial \eta}$	$f(0) = 0$	$f(1) = 0$ $f'(1) = 0$
$\underline{\mathbf{D}_\pi}$	$\frac{\partial}{\partial \eta}$	$f(0) = 0$	$f(1) = 0$ $f'(1) = 2\pi^*$
$\underline{\mathbf{DD}_p}$	$\frac{\partial^2}{\partial \eta^2}$	$f(0) = 0$ $f'(0) = 0$	$f(1) = 0$ $f'(1) = 0$
$\underline{\mathbf{I}_0^\eta}$	$\int_0^\eta$	$f'(0) = 0$ $g(0) = 0$	$f(1) = 0$ $f'(1) = 0$

There is one integral operator $\underline{\mathbf{I}_0^\eta}$ defined in Table 1. It represents integration from model top to model level η. The total integral over atmosphere $\underline{\mathbf{I}_0^1}$ is obtained when $\underline{\mathbf{I}_0^\eta}$ is evaluated on model surface ($\eta = 1$). The integral operator from model surface to model level η is defined as the difference:

$$\underline{\mathbf{I}_\eta^1} \cdot \mathbf{f} = \left(\underline{\mathbf{I}_0^1} - \underline{\mathbf{I}_0^\eta}\right) \cdot \mathbf{f}, \tag{15}$$

which represents the discrete equivalent of the additive integral property,

$$\int_\eta^1 f \, d\eta' = \int_0^1 f \, d\eta' - \int_0^\eta f \, d\eta'.$$

In the following paragraphs we describe first how the discrete representation of a continuous function known

on model η levels is obtained, and then how the vertical operators are constructed.

a. Interpolation with B-spline curve

In the process of discretizing vertical operators, we apply the FE procedure, as described for example in Lynch (2005). We use B-spline functions of a general order as the basis functions. Thus, linear functions and cubic B splines are particular choices that are consistent with the FE method used in the hydrostatic dynamical core of the ALADIN system.

First, we aim to find the input function $f(\eta)$ from the vector of known values $\mathbf{f} = (f_1, \ldots, f_L)^{\mathrm{T}}$ at full model levels and from the boundary conditions that $f(\eta)$ must satisfy according to Table 1. For this purpose, a basis of B-spline functions $a_j(\eta)$ is constructed and the function $f(\eta)$ is written as a linear combination:

$$f(\eta) = \sum_{j \in I_a} \hat{f}_j a_j(\eta), \tag{16}$$

where the coefficients $\hat{f}_j$ are found from the interpolation conditions $f(\eta_k) = f_k$ and the boundary conditions. The linear boundary conditions can be imposed on the function $f(\eta)$ in two ways. The first way, which we call *implicit*, is to define the basis functions $a_j(\eta)$ in such a way that they already satisfy the linear boundary conditions. Therefore, any linear combination of the basis functions also satisfies these conditions. The second way, which we call *explicit*, is to construct, from the expansion in (16), a linear system using the interpolation conditions $f(\eta_k) = f_k$ and the boundary conditions, and to solve this linear system providing the unknown coefficients $\hat{f}_j$. Notice that we may impose implicitly only horizontally homogeneous boundary conditions constant in time since the basis is chosen only once in the setup of the operator, and for all horizontal grid points at once. It follows that $\underline{\mathbf{D}_\pi}$ may be defined only with explicit boundary conditions. Both approaches lead to discrete representation of a given vertical operator with given boundary conditions, although these representations differ. We use explicit definitions for input boundary conditions in all experiments.

The number of basis functions, that is, the cardinal of the index I_a in (16), depends on the number of levels, the number of boundary conditions, and the method used to impose them. It is L if the *implicit* method is used, and $L + B$ if the *explicit* method is used, B being the number of boundary conditions. The actual shape of the basis functions depends on the number of levels, the boundary conditions, and the order of the B splines. In appendix A we describe in detail how basis functions are constructed.

Therefore, the function $f(\eta)$ is uniquely defined by the coefficients $\hat{\mathbf{f}}$, which in turn are determined from values of the function at full model levels $\mathbf{f}$ and the linear boundary conditions. As all the operations and conditions involved are linear, we can write a linear relation between $\mathbf{f}$ and $\hat{\mathbf{f}}$, that is, $\mathbf{f} = \underline{\mathbf{A}} \cdot \hat{\mathbf{f}}$. Moreover, the basis functions are carefully defined to ensure $\underline{\mathbf{A}}$ invertibility, and then

$$\hat{\mathbf{f}} = \underline{\mathbf{A}}^{-1} \cdot \mathbf{f}. \tag{17}$$

Once the basis functions a_j and the coefficients $\hat{\mathbf{f}}$ are specified, the relation in (16) gives the input function $f(\eta)$.

b. Vertical operator definition

The goal now is to find an output function $g(\eta)$ that represents the result of the linear operator $\mathscr{P}$ application to the input function $f(\eta)$ obtained in the previous paragraph. The output function, besides being a good approximation of $\mathscr{P}(f)$, must satisfy the output boundary conditions given in Table 1. To this end, the so-called *implicit* method is used, that is, a set of B-spline basis functions $b_j(\eta)$ that satisfies the linear boundary conditions is chosen. As already mentioned, by doing so, any linear combination of the basis functions satisfies these boundary conditions. Therefore, the candidates for the output function $g(\eta)$ are the following linear combinations:

$$g(\eta) = \sum_{j \in I_b} \hat{g}_j b_j(\eta), \tag{18}$$

where the coefficients $\hat{g}_j$ must be determined following the method of mean weighted residuals (Untch and Hortal 2004). Provided a set of arbitrary weighting functions $w_j(\eta)$ the traditional FE approach leads to the following conditions:

$$\int_0^1 \mathscr{P}(f)(\eta) w_j(\eta)\, d\eta = \int_0^1 g(\eta) w_j(\eta)\, d\eta, \tag{19}$$

for each j. When (16) and (18) are substituted into (19) and because of the linearity of the operator $\mathscr{P}$ we find

$$\underline{\mathbf{M}} \cdot \hat{\mathbf{g}} = \underline{\mathbf{S}} \cdot \hat{\mathbf{f}}, \tag{20}$$

where the mass matrix $\underline{\mathbf{M}}$ is given by

$$(\underline{\mathbf{M}})_{ij} = \int_0^1 w_i(\eta) b_j(\eta)\, d\eta, \tag{21}$$

and the stiff matrix $\underline{\mathbf{S}}$ is given by

$$(\underline{\mathbf{S}})_{ij} = \int_0^1 w_i(\eta) \mathscr{P}[a_j(\eta)]\, d\eta. \tag{22}$$

TABLE 2. The mean absolute error (MAE) of the vertical derivative operators applied on ξ for several resolutions with regularly distributed vertical levels. The accuracy order of these operators is calculated from MAE using linear regression (Calculated order). The analytically estimated accuracy orders (Analytical order), published in Staniforth and Wood (2005) for the first derivative FE operator and derived in section 4 for the second derivative FE operator, are listed in the last column. The FD derivative operator of the kth order is denoted as $\underline{\mathbf{FD}_k}$ and the FD second derivative operator of the sixth order is denoted as $\underline{\mathbf{FDD}_6}$.

Operator	MAE, No. of levels: 50	MAE, No. of levels: 100	MAE, No. of levels: 200	Calculated order	Analytical order
$\underline{\mathbf{D}_p}$	2.5×10^{-6}	8.4×10^{-9}	3.1×10^{-11}	8.15	8
$\underline{\mathbf{D}_q}$	4.1×10^{-6}	8.4×10^{-9}	3.1×10^{-11}	8.5	8
$\underline{\mathbf{FD}_8}$	1.8×10^{-6}	7.3×10^{-9}	2.9×10^{-11}	7.97	8
$\underline{\mathbf{D}_h}$	0.0029	0.00016	9.7×10^{-6}	4.21	4
$\underline{\mathbf{FD}_4}$	0.002	0.00012	7.7×10^{-6}	4.01	4
$\underline{\mathbf{FD}_2}$	0.066	0.017	0.0042	1.98	2
$\underline{\mathbf{DD}_p}$	8.8×10^{-4}	1.2×10^{-5}	1.7×10^{-7}	6.16	6
$\underline{\mathbf{FDD}_6}$	0.00057	9.2×10^{-6}	1.4×10^{-7}	5.95	6

Therefore, the output function $g(\eta)$, satisfying both (19) and the linear boundary conditions, is determined by its expansion in the basis $b_j(\eta)$, whose coefficients can be obtained from (20) by inverting the mass matrix as follows:

$$\hat{\mathbf{g}} = \underline{\mathbf{M}}^{-1} \cdot \underline{\mathbf{S}} \cdot \hat{\mathbf{f}}. \tag{23}$$

Using (18) the output function $g(\eta)$ is determined. Finally, the last step is to evaluate the output function at the output levels η'_k, that is,

$$g(\eta'_k) = \sum_{j\in I_b} \hat{g}_j \cdot b_j(\eta'_k). \tag{24}$$

This linear equation can be written in matrix form as

$$\mathbf{g} = \underline{\mathbf{B}} \cdot \hat{\mathbf{g}}, \tag{25}$$

where

$$(\underline{\mathbf{B}})_{ij} = b_j(\eta'_i). \tag{26}$$

Then, the FE matrix for the linear operator $\mathscr{P}$ is found by grouping the results given in (17), (23), and (25), that is

$$\underline{\mathbf{P}} = \underline{\mathbf{B}} \cdot \underline{\mathbf{M}}^{-1} \cdot \underline{\mathbf{S}} \cdot \underline{\mathbf{A}}^{-1}. \tag{27}$$

Matrix $\underline{\mathbf{P}}$ is a high-order approximation of the linear operator $\mathscr{P}$ for any input function f that satisfies the input linear boundary conditions such that $\mathscr{P}(f)$ satisfies the output linear boundary conditions. It must be stressed that, when applying the FE operators listed in Table 1 in the model, we must check that these operators are applied on functions that can be naturally forced to satisfy the linear boundary conditions.

In general, the operator matrix $\underline{\mathbf{P}}$ is a dense matrix. For operators in Table 1 used in the 3D simulations of section 7, the number of nonzero elements of operator matrices is above 75%. The nonlocality of the operator matrix has an impact on the efficiency of the FE method through the matrix multiplication.

4. Accuracy of vertical operators

We apply the vertical FE operators from Table 1 to the smooth function $\xi(\eta) = \sin^3(3\pi\eta)\cos(3\pi\eta)$ satisfying all the input boundary conditions listed in Table 1, except for the operator $\underline{\mathbf{D}_\pi}$ that matches $\underline{\mathbf{D}_q}$ far from boundaries. The analytic value of the integral and derivative of ξ can be easily calculated. Hence, we calculate the mean absolute error (MAE) of each FE operator for several regular distributions of η in the interval (0, 1). The achieved order of accuracy of the defined operators is then calculated through a linear regression model and listed in Table 2. The table shows as well the mean absolute errors and the analytically estimated order of accuracy of the tested operators. We denote the FD derivative operators of the kth order as $\underline{\mathbf{FD}_k}$, and the FD second derivative operator of the kth order as $\underline{\mathbf{FDD}_k}$. Vertical operators constructed with finite-element method suffer from the error close to the domain boundaries, while in the central part they show the theoretically calculated high order. Let us recall that the accuracy order of finite-difference vertical discretization currently used in the operational applications of the ALADIN system is only two for regular distribution of vertical levels and one otherwise. The mean absolute error of the current FD vertical operator for the first derivative is 4–8 orders bigger then the same error for the vertical operators designed with FE and described here. See Fig. 2 for comparison. The mean absolute error of the defined vertical operators in

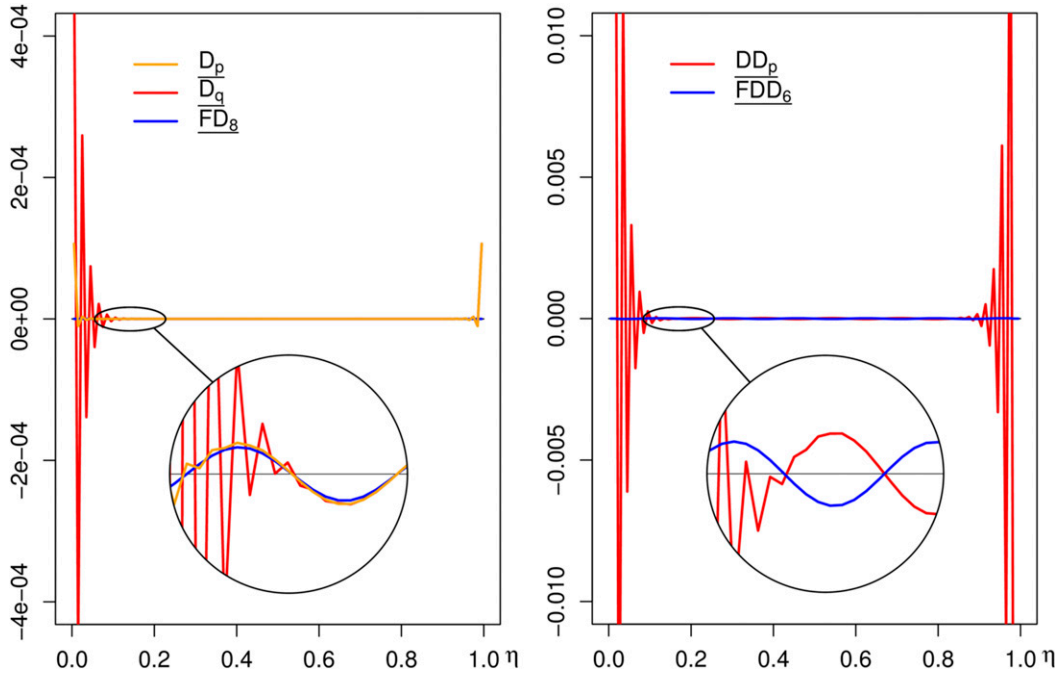

FIG. 2. The error of the defined FE vertical operators and of their FD counterparts calculated with 100 regularly distributed vertical levels, for (left) the first derivative and (right) the second derivative. We denote the eighth-order FD operator for the first derivative as $\underline{\mathbf{FD}_8}$ and the sixth-order FD operator for the second derivative as $\underline{\mathbf{FDD}_6}$.

relation to the number of vertical levels is shown in Fig. 3. The order of these operators summarized in Table 2 may be compared to ideal lines. To eliminate the boundary effects, we omit in the calculations 1/5 of the domain on each boundary.

When using cubic B splines, more than eighth-order accuracy is achieved for the integral and the first derivative operators $\underline{\mathbf{D}_p}$ and $\underline{\mathbf{D}_v}$, more than sixth order is achieved for the second derivative operator $\underline{\mathbf{DD}_p}$, and fourth order is achieved for the first derivative operator $\underline{\mathbf{D}_h}$ with the change of vertical levels distribution at the output. This property is called superconvergence and it is linked to regular model levels distribution solely. We do not show values for the vertical integral; they may be found in Untch and Hortal (2004).

The theoretical accuracy of integral and first derivative operators defined with cubic B splines was mathematically explained in Staniforth and Wood (2005). To the best of our knowledge, the same has not yet been done for a second derivative operator defined with cubic splines. We show here that the theoretical accuracy of $\underline{\mathbf{DD}_p}$ is 6.

We assume regular η level distribution with distance $\Delta\eta = h$. We follow the process described in section 3b to approximate $g = \mathscr{P}(f) = \partial^2 f/\partial\eta^2$. Let $\hat{\mathbf{f}}$ and $\hat{\mathbf{g}}$ be the coefficients of the linear transformations (16) and (18) and let $\mathbf{f}$ and $\mathbf{g}$ be values of f and g at full model levels. Let us consider full model levels far enough from the domain top and bottom boundaries.

We use the following equalities

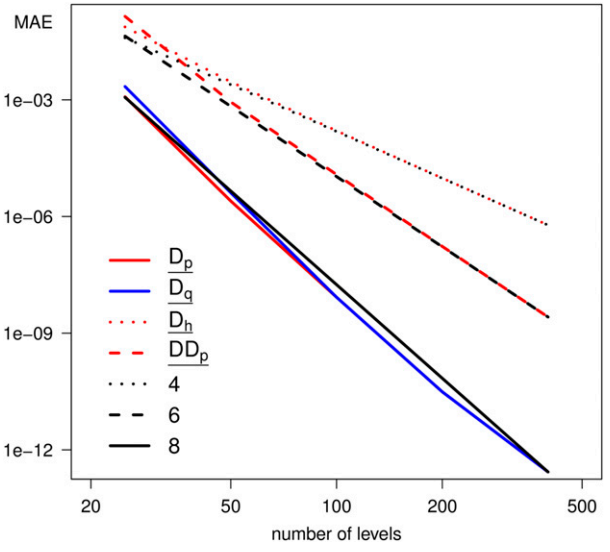

FIG. 3. The mean absolute error of the defined vertical operators in relation to the number of vertical levels. Black lines show ideal line corresponding to the order 4, 6, and 8. The ideal line is followed almost exactly with FD operators of the corresponding order (not shown).

$$\frac{1}{5040}(\hat{g}_{k+3}+120\hat{g}_{k+2}+1191\hat{g}_{k+1}+2416+1191\hat{g}_{k-1}+120\hat{g}_{k-2}+\hat{g}_{k-3})$$
$$=\frac{1}{120h^2}(\hat{f}_{k+3}+24\hat{f}_{k+2}+15\hat{f}_{k+1}-80+15\hat{f}_{k-1}+24\hat{f}_{k-2}+\hat{f}_{k-3}), \tag{28}$$

$$\frac{1}{5040}\left(\frac{g_{k+3}+g_{k-3}}{2}+120\frac{g_{k+2}+g_{k-2}}{2}+1191\frac{g_{k+1}+g_{k-1}}{2}+1208\right)$$
$$=\frac{1}{120h^2}\left(\frac{f_{k+3}+f_{k-3}}{2}+24\frac{f_{k+2}+f_{k-2}}{2}+15\frac{f_{k+1}+f_{k-1}}{2}-40\right), \tag{29}$$

$$(mh)^2[\cos(3mh)+120\cos(2mh)+1191\cos(mh)+1208]\widetilde{g_m}$$
$$=42m^2[\cos(3mh)+24\cos(2mh)+15\cos(mh)-40]\widetilde{f_m}. \tag{30}$$

First, we express the kth element of (20) using (21) and (22) and cubic spline basis functions $a_j(\eta)$ and $b_j(\eta)$ to get (28). Far from domain top and bottom boundaries, the transformations (16) and (18) may be written as

$$f_k=f(\eta_k)=\frac{1}{6}\left(\hat{f}_{k+1}+4\hat{f}_k+\hat{f}_{k-1}\right),$$
$$g_k=g(\eta_k)=\frac{1}{6}\left(\hat{g}_{k+1}+4\hat{g}_k+\hat{g}_{k-1}\right).$$

Thus, a weighted combination of (28) evaluated at $k-1$, k, and $k+1$ gives (29) for the full level values **f** and **g**.

The truncation error may then be determined by the Taylor expansion of the Fourier series proceeding in the similar way to Staniforth and Wood (2005). We expand (f_k, g_k) as $(f_k, g_k)=(\widetilde{f_m}, \widetilde{g_m})\exp(imkh)$, where m is a wavenumber and $\widetilde{f_m}$ and $\widetilde{g_m}$ are the coefficients of the discrete Fourier expansion of f_k and g_k, respectively. It yields (30). We approximate by the Taylor series and simplify as follows:

$$\frac{42[\cos(3mh)+24\cos(2mh)+15\cos(mh)-40]}{(mh)^2[\cos(3mh)+120\cos(2mh)+1191\cos(mh)+1208]}$$
$$\approx -1-\frac{m^6h^6}{30\,240}+\mathcal{O}(m^8h^8).$$

Finally, for the discrete Fourier expansion coefficients we get

$$\widetilde{g_m}=-m^2\widetilde{f_m}\left[1+\frac{m^6h^6}{30\,240}+\mathcal{O}(h^8)\right]$$

giving the expected sixth-order accuracy of the second derivative operator g denoted $\underline{\mathbf{DD}_p}$ in Table 1.

5. Time stepping

a. Linear system

The dynamical core of the ALADIN system uses the Z grid as described in Caluwaerts et al. (2015). The horizontal momentum equation (2) is reformulated in the linear model used by the semi-implicit time stepping in terms of horizontal divergence D and relative vorticity ζ:

$$D=\frac{\partial u}{\partial x}+\frac{\partial v}{\partial y}$$
$$\xi=\frac{\partial v}{\partial x}-\frac{\partial u}{\partial y}. \tag{31}$$

For stability reasons described in Bénard (2003) and Bénard et al. (2004, 2005) also the vertical momentum equation (3) is transformed into vertical divergence d defined as

$$d=-g\frac{p}{mRT}\frac{\partial w}{\partial \eta}+\frac{p}{mRT}\nabla\phi\cdot\frac{\partial V}{\partial \eta}. \tag{32}$$

Thereby the full implicit treatment of the tridimensional divergence term (8) is achieved, since it becomes the linear combination of prognostic variables as follows:

$$D_3=D+d. \tag{33}$$

On the other hand, there is no semi-implicit correction of vorticity in spectral space. Only the divergent part of the flow is corrected under our assumptions used in the linear model definition (Bénard et al. 2010). The transformation (31) and its inverse is carried out in spectral space of the ALADIN system. However, this is not admissible for the vertical part as (32) is nonlinear. Hence, the transformations between w and d

must be done in gridpoint space. Right after inverse Fourier transformations we retrieve w from d. Then an explicit guess of all prognostic quantities is computed using the time explicit semi-Lagrangian scheme. It allows us to recover an explicit guess of d using (32). Finally we add to the explicit guess the missing terms related to the semi-implicit part of the computation and then the total forcing terms of the prognostic quantities (V, d, T, $\hat{q}$, q_s) are transformed into spectral space where the implicit problem is solved.

The transformation of prognostic variables between spectral and gridpoint space is not a physical process. It should not contribute to the time evolution of quantities under transformations. This means that the vertical integral operator used when going from d to w must be the inverse of the vertical derivative operator used in the opposite direction. To define relevant FE operators ensuring this property is a cumbersome problem and we have not succeeded in formulating such operators while preserving stability properties. For that reason, w to d transformation and d to w backward transformation are done with FD operators $\underline{\mathbf{T}_d}$ and $\underline{\mathbf{T}_w}$, respectively, with prognostic quantity w being placed on half model levels (Lorenz 1960). Indeed, $\underline{\mathbf{T}_w}$ is a discrete representation of an integral from the surface to the η level, while $\underline{\mathbf{T}_d}$ represents vertical derivative along η. For a function $\mathbf{f} = (f_1, \ldots, f_L)^{\mathrm{T}}$ defined on full model levels and a function $\mathbf{g} = (g_{\bar{1}}, \ldots, g_{\bar{L}})^{\mathrm{T}}$ defined on half model levels, we may write

$$\left(\underline{\mathbf{T}_w} \cdot \mathbf{mf}\right)_{\bar{l}} = g_s + \sum_{k=l+1}^{L} f_k \delta\pi_k, \tag{34}$$

$$\left(\frac{1}{\mathbf{m}}\underline{\mathbf{T}_d} \cdot \mathbf{g}\right)_l = \frac{g_{\bar{l}} - g_{\widetilde{l-1}}}{\delta\pi_l}, \tag{35}$$

where $\delta\pi_k$ is defined by (C2) in appendix C and g_s represents the bottom boundary condition that has to be specified before transformation. Since $\mathbf{g} = \mathbf{w}$ in our case we use (11) as the bottom boundary condition. Notice that the resulting functions are defined on half model levels and full model levels, respectively.

The linear system in terms of prognostic variables (D, d, T, $\hat{q}$, q_s) is obtained by traditional linearization around the reference atmosphere at rest, hydrostatically balanced, dry, isothermal, and with no orography (Bubnová et al. 1995; Bénard et al. 2010). The reference atmosphere is then given by two parameters only: T^* representing temperature and π_s^* representing surface pressure. The stability of the semi-implicit scheme depends strongly on T^* and π_s^*. Because of stability reasons a coefficient $r \leq 1$ is used within the linear model (Bénard 2004). The linear system then writes

$$\frac{\partial D}{\partial t} = -R\mathscr{G}\Delta T + RT^*\left[(\mathscr{G} - 1)\Delta\hat{q} - \Delta q_s\right], \tag{36}$$

$$\frac{\partial d}{\partial t} = -\frac{g^2}{rRT^*}\mathscr{L}\,\hat{q}, \tag{37}$$

$$\frac{\partial T}{\partial t} = -\frac{RT^*}{C_v}(D + d), \tag{38}$$

$$\frac{\partial \hat{q}}{\partial t} = \mathscr{S}D - \frac{C_p}{C_v}(D + d), \tag{39}$$

$$\frac{\partial q_s}{\partial t} = -\mathscr{N}D, \tag{40}$$

where Δ is the horizontal Laplacian and the linear operators ∂, $\mathscr{G}$, $\mathscr{S}$, and $\mathscr{N}$ are defined in Bubnová et al. (1995) as

$$\partial(f) = \frac{\pi^*}{m^*}\frac{\partial f}{\partial \eta}, \tag{41}$$

$$\mathscr{G}(f) = \int_{\eta}^{1} \frac{m^*}{\pi^*} f\, d\eta', \tag{42}$$

$$\mathscr{S}(f) = \frac{1}{\pi^*}\int_{0}^{\eta} m^* f\, d\eta', \tag{43}$$

$$\mathscr{N}(f) = \frac{1}{\pi_s^*}\int_{0}^{1} m^* f\, d\eta', \tag{44}$$

where $\pi^*(\eta) = A(\eta) + B(\eta)\pi_s^*$ is the hydrostatic pressure of the reference atmosphere and $m^*(\eta) = \partial\pi^*(\eta)/\partial\eta$ is the metric term.

Discretization of the vertical integral operators $\mathscr{G}, \mathscr{S}$, and $\mathscr{N}$ is straightforward. We first define $\boldsymbol{\pi}^*$ as the discrete version of $\pi^*(\eta)$, that is, the reference hydrostatic pressure evaluated at full model levels. Similarly we define $\mathbf{m}^*$ from $m^*(\eta)$.

Then, the discrete versions of the operators $\mathscr{G}, \mathscr{S}$, and $\mathscr{N}$ are, respectively,

$$\underline{\mathbf{G}} \cdot \mathbf{f} = \underline{\mathbf{l}_{\eta}^{1}} \cdot \left(\frac{\mathbf{m}^*}{\boldsymbol{\pi}^*}\mathbf{f}\right), \tag{45}$$

$$\underline{\mathbf{S}} \cdot \mathbf{f} = \frac{1}{\boldsymbol{\pi}^*}\underline{\mathbf{l}_{0}^{\eta}} \cdot (\mathbf{m}^*\mathbf{f}), \tag{46}$$

$$\underline{\mathbf{N}} \cdot \mathbf{f} = \frac{1}{\pi_s^*}\underline{\mathbf{l}_{0}^{1}} \cdot (\mathbf{m}^*\mathbf{f}). \tag{47}$$

The vertical Laplacian is given by

$$\mathscr{L}(f) = \partial(1 + \partial)(f), \tag{48}$$

and its discretization is more cumbersome. For stability reasons, we reformulate it in the continuous form to

$$\mathscr{L}(f) = \frac{1}{m^*}\frac{\partial}{\partial\eta}\left(\frac{\pi^{*2}}{m^*}\right)\frac{\partial f}{\partial\eta} + \left(\frac{\pi^*}{m^*}\right)^2\frac{\partial^2 f}{\partial\eta^2}, \tag{49}$$

and substitute vertical derivatives using the discrete FE operators $\underline{\mathbf{D}_p}$, $\underline{\mathbf{D}_\pi}$, and $\underline{\mathbf{DD}_p}$. Finally, the discrete Laplacian operator is given by

$$\underline{\mathbf{L}} \cdot \mathbf{f} = \frac{1}{\mathbf{m}*}\left[\underline{\mathbf{D}_\pi} \cdot \left(\frac{\boldsymbol{\pi}^{*2}}{\mathbf{m}*}\right)\right]\left(\underline{\mathbf{D}_p} \cdot \mathbf{f}\right) + \left(\frac{\boldsymbol{\pi}^*}{\mathbf{m}*}\right)^2\left(\underline{\mathbf{DD}_p} \cdot \mathbf{f}\right). \tag{50}$$

b. Implicit problem

In the semi-implicit scheme of the ALADIN system with the FD method used in the vertical, a single Helmholtz equation is solved in the spectral space. This equation is reached by a suitable algebraic elimination of all variables but one, namely, d. There is a mathematical constraint, called C1, which enables such elimination, and it writes

$$\mathscr{GS} - \mathscr{S} - \mathscr{G} + \mathscr{N} = 0. \tag{51}$$

Unfortunately, this constraint is not fulfilled for the FE operators used in the vertical discretization. On the other hand, the implicit problem in the discrete form is a linear inversion, and could be performed with two or more variables. If we adopt a solution of the implicit problem for the couple (D, d), then the constraint C1 no longer needs to be fulfilled. Instead of solving a system of L equations for the variable d, the Helmholtz equation, we can solve a system of $2L$ equations for the couple (D, d). However, solving this equation by direct inversion has particular memory requirements. This is because we should invert, in the setup of the model, a considerable big set of matrices, one for each pair of spectral wavenumbers, and store them during the whole integration.

Therefore, instead of a direct inversion, we have opted for a preconditioned iterative method, which we outline in appendix B.

c. Nonlinear system

The vertically discretized fully compressible Euler equations are written as follows:

$$\frac{d\mathbf{V}}{dt} = -\frac{R\mathbf{T}}{\mathbf{p}}\nabla\mathbf{p} - \left(\frac{\mathbf{p}}{\boldsymbol{\pi}} + \frac{\mathbf{p}}{\mathbf{m}} \cdot \underline{\mathbf{D}_q} \cdot \hat{\mathbf{q}}\right) \cdot \nabla\boldsymbol{\phi}, \tag{52}$$

$$\frac{d\mathbf{T}}{dt} = -\frac{R\mathbf{T}}{C_v}\mathbf{D}_3, \tag{53}$$

$$\frac{d\hat{\mathbf{q}}}{dt} = -\frac{C_p}{C_v}\mathbf{D}_3 - \frac{\boldsymbol{\omega}}{\boldsymbol{\pi}}, \tag{54}$$

$$\frac{\partial q_s}{\partial t} = -\frac{1}{\pi_s}\underline{\mathbf{l}_0^1} \cdot (\nabla \cdot (\mathbf{mV})). \tag{55}$$

These equations are evaluated at full model levels, while the equation for vertical velocity is evaluated at half model levels, since it is a half-level quantity. For this reason, we need FE operator for the first derivative, denoted $\underline{\mathbf{D}_h}$, which gives values of the first derivative on the half model levels, when it is applied to a full-level variable. Then

$$\frac{d\mathbf{w}}{dt} = \frac{g}{\mathbf{m}_h}\underline{\mathbf{D}_h} \cdot (\mathbf{p} - \boldsymbol{\pi}), \tag{56}$$

where $\mathbf{m}_h$ is a discrete representation of $m(\eta)$ on half model levels computed as

$$(\mathbf{m}_h)_l = \frac{\pi_{l+1} - \pi_l}{\eta_{l+1} - \eta_l}. \tag{57}$$

The terms $\nabla\boldsymbol{\phi}$, $\mathbf{D}_3$, and $\boldsymbol{\omega}$ further include vertical operators and are hence affected by the choice of vertical discretization. The total divergence and the geopotential horizontal gradient are discretized from their continuous definitions (8) and (9) as

$$\mathbf{D}_3 = \mathbf{D} - \frac{\mathbf{p}}{\mathbf{m}R\mathbf{T}}\left(\underline{\mathbf{T}_d} \cdot g\mathbf{w} - \nabla\boldsymbol{\phi}\underline{\mathbf{D}_p} \cdot \mathbf{V}\right), \tag{58}$$

$$\nabla\boldsymbol{\phi} = \nabla\phi_s + \underline{\mathbf{l}_\eta^1} \cdot \nabla\left(\frac{\mathbf{m}R\mathbf{T}}{\mathbf{p}}\right), \tag{59}$$

and, finally, the total time derivative of the hydrostatic pressure is discretized from (7) as

$$\boldsymbol{\omega} = \mathbf{V} \cdot \nabla\boldsymbol{\pi} - \underline{\mathbf{l}_0^\eta} \cdot (\nabla \cdot (\mathbf{mV})). \tag{60}$$

To calculate the advection of w in (56), we need to evaluate w at half model levels using the definition (32) through

$$\mathbf{w} = -\frac{1}{g}\underline{\mathbf{T}_w} \cdot \left(\mathbf{m}\frac{R\mathbf{T}}{\mathbf{p}}\mathbf{d} - \nabla\boldsymbol{\phi}\underline{\mathbf{D}_p} \cdot \mathbf{V}\right) \tag{61}$$

and use the standard interpolation procedure applied in the semi-Lagrangian advection scheme.

It was shown in Guerra and Ullrich (2016) that unstaggered FE method results possess highly oscillatory stationary computational modes that pollute the solution. Let us mention that FE operators $\underline{\mathbf{D}_d}$ and $\underline{\mathbf{I}_w}$ could be defined instead of $\underline{\mathbf{T}_d}$ and $\underline{\mathbf{T}_w}$, keeping staggering of variables in the vertical. In such case, $\underline{\mathbf{D}_d}$ gives values on full model levels when applied on half model level variables and $\underline{\mathbf{I}_w}$ gives values on half model levels when applied on full model level variables. To avoid artificial forcing coming from transformations of vertical velocity w to vertical divergence d and vice versa, the operators $\underline{\mathbf{D}_d}$ and $\underline{\mathbf{I}_w}$ have to be the inverse of each other according to

$$\mathbf{f} = \underline{\mathbf{D}_d} \cdot \underline{\mathbf{I}_w} \cdot \mathbf{f}, \tag{62}$$

$$\mathbf{f} = \underline{\mathbf{I}_w} \cdot \underline{\mathbf{D}_d} \cdot \mathbf{f}, \tag{63}$$

for each discrete function **f**. Our attempt to define such operators unfortunately resulted in noisy solutions of the basic tests described in the next section.

6. Sensitivity in idealized experiments

A set of test cases has been run in the 2D vertical plane version of the ALADIN system, including the nonlinear nonhydrostatic flow over idealized orography according to Bubnová et al. (1995) and the density current test published in Straka et al. (1993).

a. *Nonlinear nonhydrostatic flow*

First, we examine flows with a constant uniform velocity $U = 4\,\mathrm{m\,s^{-1}}$ in the x direction in a dry atmosphere with the temperature profile determined by a constant Brunt–Väisälä frequency $N = 0.01\,\mathrm{s^{-1}}$ and the bottom temperature $T_0 = 285\,\mathrm{K}$ over a bell-shaped mountain characterized by its height H and its half-width a. The surface geopotential is defined by

$$\Phi_s(x) = gH\frac{a^2}{a^2 + x^2}. \tag{64}$$

We set $H = a = 400\,\mathrm{m} = 5\Delta x$. We have 384 grid points in the x direction with $\Delta x = 80\,\mathrm{m}$. We use 140 regularly spaced vertical model levels with $\Delta z = 180\,\mathrm{m}$. An additional 10 levels are placed at the top of the model domain to allow a smooth transition up to the model top defined by $\pi = 0\,\mathrm{Pa}$. The top 20 levels are kept isothermal with a temperature of 102 K. We use the time step $\delta t = 4\,\mathrm{s}$ and integrate up to 5000 s. The semi-implicit two time level time stepping (Hortal 2002) is applied, without any artificial dissipation algorithm like sponge, diffusion, or time decentering. The results for the vertical velocity field for the two vertical discretizations, FD and FE with cubic B splines, are shown in Fig. 4. Both results are in good agreement not showing signs of apparent instability.

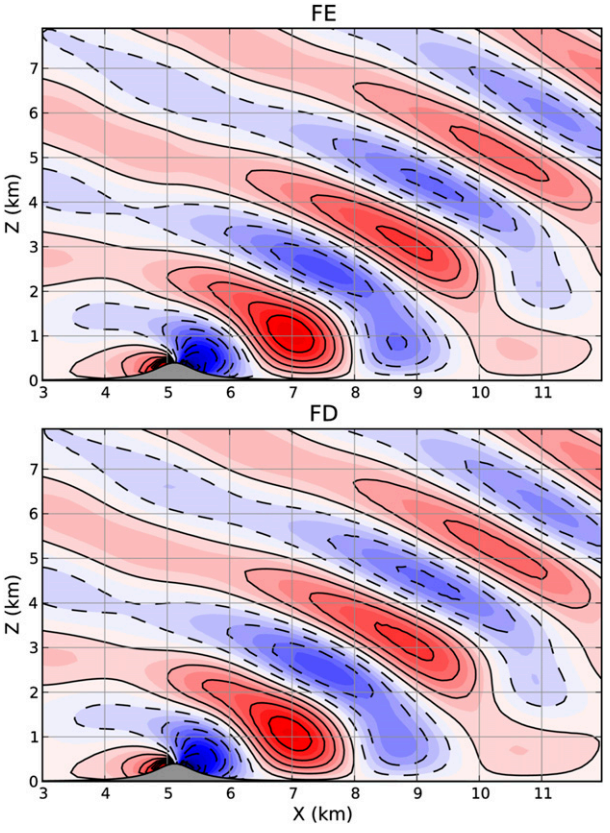

FIG. 4. Vertical velocity at time 5000 s for the nonlinear mountain wave. The contour interval is $0.2\,\mathrm{m\,s^{-1}}$. The results are shown for (top) the FE vertical discretization and (bottom) the FD vertical discretization.

b. *Density current*

We apply the same initial configuration as in Straka et al. (1993) for comparison. We first run the reference experiment with high horizontal and vertical spatial resolution $\Delta x = \Delta z = 25\,\mathrm{m}$ and with a short time step of 0.1 s. Then two sets of runs are prepared with a longer time step of 2 s. The first one has the same horizontal and vertical resolution as the reference experiment, and the second one uses the coarser horizontal and vertical resolution of 50 m. Other parameters are kept from the reference solution. The horizontal domain length is 51.2 km. In the vertical, the model levels are placed regularly up to 4 km and then there is a transition zone of 40 model levels with a smoothly increasing vertical resolution up to 25 km. The top seven levels are set to be isothermal. To initiate a density current, the temperature field is specified as a sum of the background value calculated from the constant potential temperature $\theta_0 = 300\,\mathrm{K}$ and a temperature perturbation $T'(x, z)$ symmetric around a central point (x_c, z_c) with a maximum value of $T_0 = 15\,\mathrm{K}$ according to the following definition:

$$T(x,z) = \theta_0\left(\frac{\pi_s}{\pi_0}\right)^{R/C_p} + T'(x,z),$$

where the perturbation temperature is defined as

$$T'(x,z) = \begin{cases} 0 & \text{for} \quad L > 1 \\ T_0[\cos(\pi L) + 1]/2 & \text{for} \quad L \le 1 \end{cases}$$

with

$$L = \sqrt{\left(\frac{x - x_c}{x_r}\right)^2 + \left(\frac{z - z_c}{z_r}\right)^2},$$

and $\pi_0 = 1000\,\text{hPa}, x_c = 2560\,\text{m}, x_r = 4000\,\text{m}, z_c = 3000\,\text{m}$, and $z_r = 2000\,\text{m}$. The semi-implicit two time level time stepping is applied. Periodic boundary conditions are imposed in the horizontal direction. The results of the described experiments with the two vertical discretizations used are shown in Fig. 5. The plotted field is the potential temperature at time 600 s. Only a part of the right half of the domain is depicted.

All basic features of the solution are kept by both methods. Compared with the reference solution, the details are better captured by the FE method. For a grid spacing of 25 m (Figs. 5b,c) the FE method gives a better shape of all the rotors than the FD method, and for a grid spacing of 50 m (Figs. 5d,e) the depth of the rotors is better resolved by the FE than the FD method. All results are in good agreement with the results shown in Fig. 1 of Straka et al. (1993).

7. Sensitivity in real-case experiments

Two series of forecasts starting from the ALARO[1] analysis at 0000 UTC were run in 2-km horizontal resolution over the central Europe domain centered above the Czech Republic and partially covering the Alps (see Fig. 6) with 87 Czech operational vertical levels. One set starts from 28 May 2016 and continues to 6 June 2016 with convection events present frequently during the day over the majority of the domain. The second set covers the time period starting from 21 October to 30 October 2017. The conditions were stable with very strong wind occurring on 29 October 2017 with wind gusts exceeding 45 m s^{-1}. The forecast integration range is 24 h with a 1-h coupling interval, the lateral boundary information is provided by the Czech operational suite of ALARO at 4.7-km horizontal resolution. We use two time level iterative centered-implicit time schemes with one iteration and the time step of 72 s. As a parameterization package, the ALARO physics is employed as described in Termonia et al. (2018), with the Modular Multiscale Microphysics and Transport (3MT) moist deep convection scheme overcoming the problem of partially resolved deep cumulus, with the radiation scheme Actif Calcul de Rayonnement et Nébulosité, version 2 (ACRANEB) and with the turbulence model II of Third Order moments Unified Condensation And N-dependent Solver (TOUCANS).

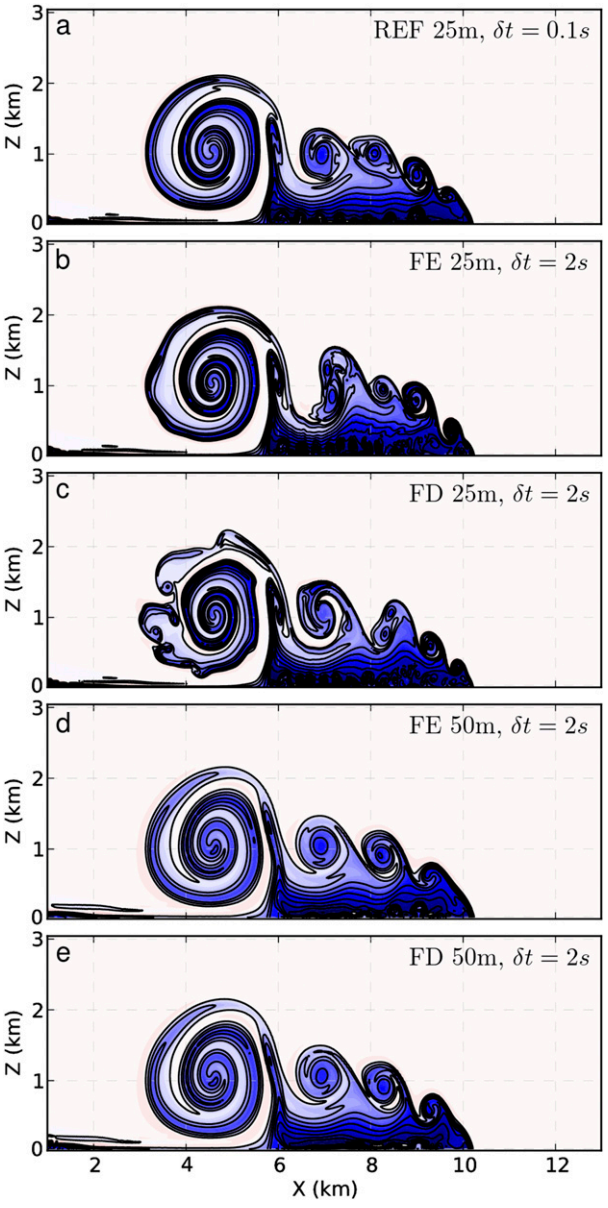

FIG. 5. The potential temperature field at time 600 s of the Straka test, the contour interval is 1 K. (a) The reference FD, (b) FE with a spatial resolution of 25 m, (c) FD with a spatial resolution of 25 m, (d) FE with a spatial resolution of 50 m, and (e) FD with a spatial resolution of 50 m. The time step in the reference solution is 0.1 s, and in all other experiments it is 2 s.

No sign of instability is apparent in any of the experiments. The iterative semi-implicit solver converges as indicated by the spectral radius test of the iteration matrix calculated in the setup part of the integration. Objective scores of the results with 1 iteration and with 10 iterations coincide in all parameters except for the

[1] ALARO is the canonical model configuration of the ALADIN system, as described in Termonia et al. (2018).

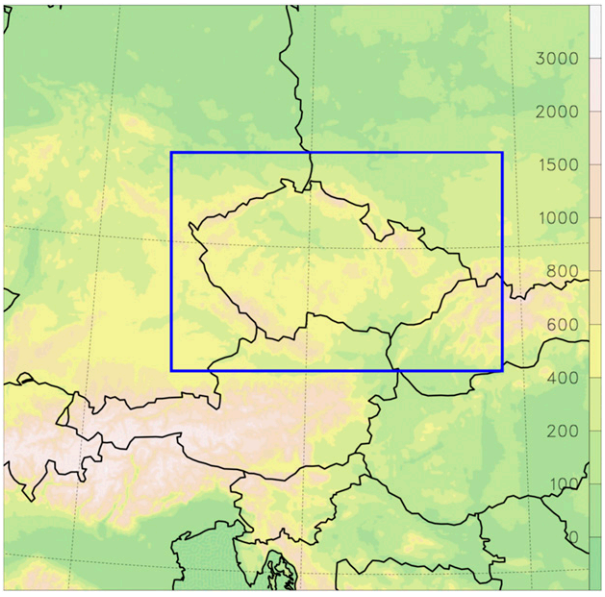

FIG. 6. Orography in real experiments. The blue rectangle denotes the domain for cumulated precipitation shown in Fig. 7.

time evolution of the bias for precipitation cumulated for 24 h in the autumnal series, where a small advantage of further iterations may be observed. We conclude that one iteration of the semi-implicit solver is enough for an accurate solution.

Furthermore, objective score characteristics are neutral to the change of vertical discretization (from FD to FE). The phenomenon that can be identified in the results is an interaction of the vertical discretization with the resolved convection. Just for providing an example, the precipitation cumulated for 3 h between 1100 and 1400 UTC is shown in Fig. 7 for the integration starting at 0000 UTC 1 June 2016. The maxima are decreased slightly with FE discretization, which corresponds better to observations.

The computational performance depends heavily on the computational platform used. The 3D experiments for this paper were run on NEC LX series HPC cluster with 320 computing nodes, with each node based on two Intel Broadwell CPUs. For any configuration, the FE method is more expensive then the FD method. The computational overhead of the FE method depends nevertheless on the used hybrid parallelization (MPI-OpenMP), nodes usage, and on the cash-blocking mechanism realized through the cash-blocking length parameter. We show in Table 3 the average CPU time needed for one time step of the whole model integration for several cash-blocking lengths. The results obtained are dependent on other computer device parameters as well and the conclusions on the CPU time consumption are only illustrative.

The average CPU time overhead of the FE method over the FD method was calculated using the average

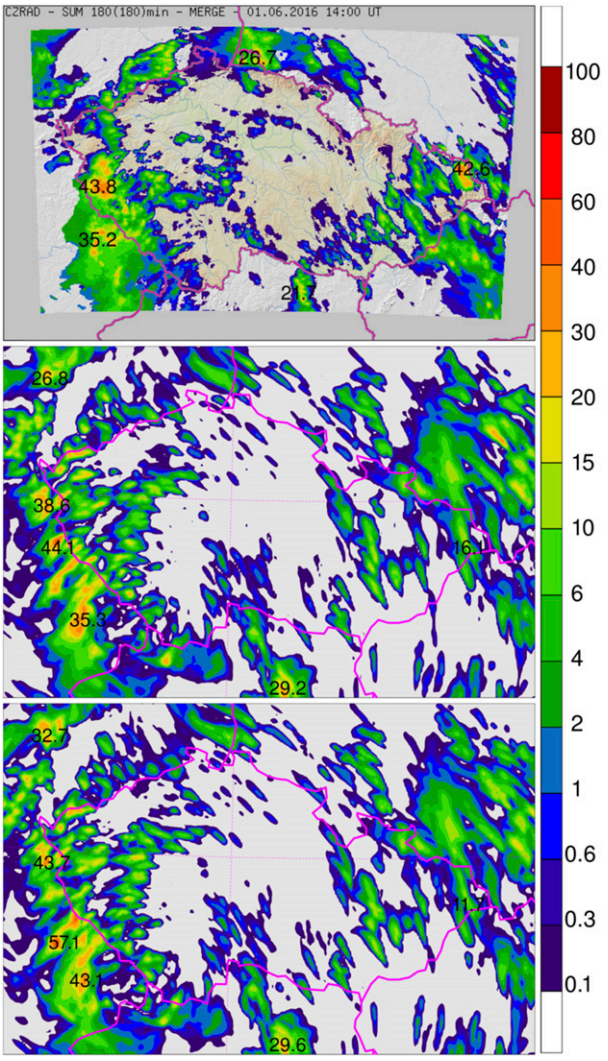

FIG. 7. Estimation of precipitation cumulated at 1100–1400 UTC 1 Jun 2016 over the Czech republic territory. (top) Combined information from radars and point rain gauges and the corresponding precipitation field forecasted by the ALARO simulation with the vertical discretization realized (middle) through FE and (bottom) through FD. Only one iteration of the semi-implicit solver is applied in both cases.

CPU time per one time step. Without iteration of the Helmholtz solver, the overhead comes from the matrix multiplication employed in the FE method in place of the difference and division operations used in the FD method. It depends on the matrix multiplication code efficiency. We use FORTRAN routine DGEMM from the Lapack library for matrix multiplication. The magnitude of this overhead is 5%–8%. Moreover, there is an overhead of needed CPU time for the FE method coming from different methods used in the Helmholtz solver and depending on the number of iterations of this solver. The magnitude of this overhead is about 1%–2%

TABLE 3. The average CPU time needed for one time step of the 3D simulation for the two vertical discretization methods, the average CPU time overhead of the FE method without iteration of the Helmholz solver, and the average CPU time overhead of the Helmholtz solver iterations over the FD method in percent units. Here "0 + 1" denotes CPU time overhead of the FE solution used in 3D experiments over the FD solution. Different cash-blocking lengths are applied. The 3D experiments were run on 72 computing nodes of the NEC LX series HPC cluster, each node is based on two Intel Broadwell CPUs.

	CPU time (s)					CPU time overhead (%)				
	FD	FE	FE	FE	FE	FE				
	No. of iterations					No. of iterations				
Cash-blocking length	0	0	1	2	5	0	1	2	5	0 + 1
120	0.814	0.874	0.889	0.906	0.963	0.0735	0.0188	0.0403	0.1099	0.0922
160	0.739	0.779	0.795	0.813	0.865	0.0548	0.0215	0.0454	0.1163	0.0763
200	0.809	0.863	0.879	0.899	0.950	0.0675	0.0189	0.0435	0.1073	0.0864
720	1.428	1.539	1.551	1.584	1.617	0.0780	0.0083	0.0313	0.0548	0.0863
1600	1.712	1.848	1.862	1.828	1.906	0.0792	0.0081	−0.0117	0.0342	0.0873

per iteration (one iteration is enough to reach satisfactory results).

The overall CPU time needed is thus increased by 8%–9% when the FE method is used (the last column in Table 3 denoted "0 + 1") depending on the parallelization (MPI-OpenMP) and the optimization method applied. The important fact is that the CPU time needed is independent of the order of B splines used as basis functions. On the other hand, increasing the order of the FD vertical discretization would lead to the increase in CPU time consumption.

8. Summary and discussion

We describe in this work a finite-element vertical discretization used in the nonhydrostatic fully compressible dynamical core of the ALADIN system, which is general in the order of used B splines. The described method is an extension and generalization of the FE method implemented for the vertical discretization of the hydrostatic dynamical core of the ALADIN system and of ARPEGE/IFS global weather prediction system described in Untch and Hortal (2004).

The treatment of boundary conditions was changed with respect to the FE implementation in the hydrostatic core of the ALADIN system. We have included, in the definition of the FE operators, a set of linear boundary conditions that are applied to the input and output functions. We found out that the boundary conditions are crucial to achieve satisfactory stability properties. Nevertheless, the conditions imposed on the input and output functions are fully compatible with physical criteria valid for the corresponding meteorological variable.

In addition, compared to FD spectral space computations, we have implemented a stationary iterative solution of the Helmholtz structure equation. The proposed method appears to be convergent and it was shown that one iteration provides sufficient accuracy.

We performed a set of standard idealized tests, like the density current Straka test and various flow regimes over a bell-shaped mountain. These experiments proved the satisfactory accuracy properties of the proposed FE discretization, and they showed that the nonhydrostatic dynamical core remains as stable as it is with the FD discretization used in the vertical when semi-implicit time stepping is applied. Moreover, 3D diabatic experiments were performed with a 2-km model horizontal resolution over the central Europe domain partially covering the Alps. The objective scores were neutral to the change of vertical discretization in all tested cases. A slight shift of the precipitation amounts to lower intensities was observed with the FE method used, especially in the summer period.

The stability properties of the NH dynamical core require us to keep vertical staggering of the model variables for FE discretization. Hence, unlike all the other prognostic variables, the vertical velocity w is defined on the half model levels. The vertical derivative of w then requires an application of a staggered FE operator. This requirement limits the theoretical accuracy of the proposed FE method, because staggered FE operators are not superconvergent. Moreover, the transformations between w and the vertical divergence variable d needed in the implicit calculations keep the FD approach. This may again limit the possible overall accuracy of the model. This is left for further investigation.

We have implemented the FE method with the general order of B splines. So far all tests were restricted to the cubic B splines only. Nevertheless, we plan to study the influence of the B-spline order on the accuracy and the time stepping stability of the whole system.

Acknowledgments. The authors express their gratitude to all the ALADIN and HIRLAM colleagues involved in the development of the ALADIN-HIRLAM system

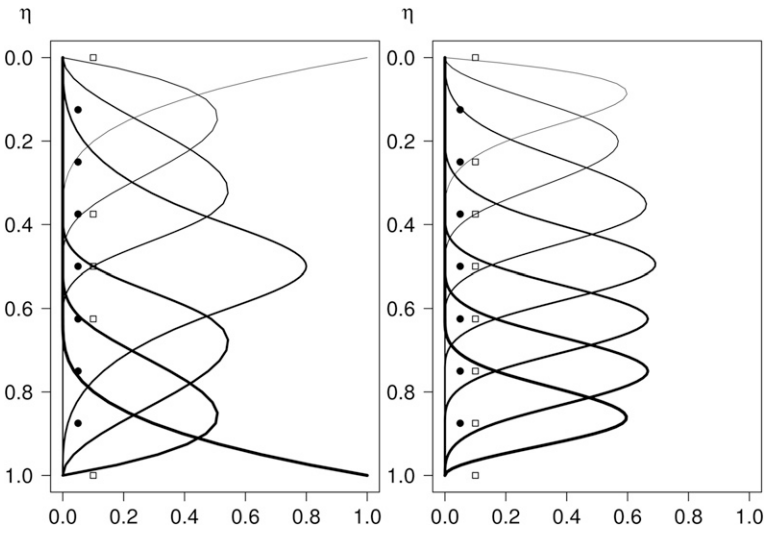

FIG. A1. A different basis for seven vertical model levels. Black dots denote vertical η levels, while squares indicate positions of knots. The thickness of lines differs for individual basis functions to better distinguish between them. (left) No boundary conditions applied and (right) three boundary conditions applied implicitly: $a_i(0) = 0$ for the top and $a_i(1) = a_i'(1) = 0$ for the bottom, $i = 1, 2, \ldots, 7$.

for their support. We would like to give special thanks to Álvaro Subías for fruitful discussions and Karim Yessad for his work on several parts of the semi-implicit time scheme facilitating our work. We are grateful to RC LACE for the financial support of several research stays devoted to the topic of this paper. We further thank the two anonymous reviewers whose suggestions helped improve and clarify the manuscript.

APPENDIX A

Construction of B-Spline Basis Functions

In this appendix we explain how the B-spline basis functions are constructed. The goal is to construct a B-spline basis function $a_k(\eta)$ that, optionally, satisfies some linear boundary properties.

The input information is the order C of the B splines ($C = 4$ for cubic splines), the number B of linear boundary conditions ($B = 0$ if no conditions are imposed), and the values of the functions $A(\eta)$ and $B(\eta)$ at the L full model levels, that is, A_k and B_k for $k = 1, 2, \ldots, L$.

First, we define the value of the vertical coordinate η at full model levels as follows:

$$\eta_k = \frac{A_k}{\pi_s^*} + B_k, \tag{A1}$$

where π_s^* is the reference hydrostatic pressure on the surface. Observe that $\eta = 0$ at the top of the atmosphere, in the limit that pressure tends to zero, and $\eta = 1$ on the surface.

We must define some η points, referred to as the knots, which may be different from the η values at the full model levels. However, once the distribution of the full model levels is given, the choice of knots is not arbitrary, because B-spline basis functions must be distributed in such a way that there is at least one full model level in the support of each B-spline function. Once the knots are set, the B-spline basis functions are constructed from them using de Boor's algorithm (de Boor 1978).

The number of knots is $L + B + C$. They are defined as follows: there is one knot at $\eta = 0$ with multiplicity C, and one other knot at $\eta = 1$ with the same multiplicity. The other $L + B - C$ knots are placed at full model levels, removing, if needed, the outermost knots. For instance, if $C = 4$, $B = 0$, and $L = 7$ we set the 11 knots as $(0, 0, 0, 0, \eta_3, \eta_4, \eta_5, 1, 1, 1, 1)$. If we impose three boundary conditions, $B = 3$ and 14 knots are set as $(0, 0, 0, 0, \eta_2, \eta_3, \eta_4, \eta_5, \eta_6, \eta_7, 1, 1, 1, 1)$. These examples are illustrated in Figure A1.

APPENDIX B

Iterative Procedure to Solve the Helmholtz Problem

The iterative procedure designed to solve the Helmholtz problem when elimination of all the prognostic variables but one (namely d) is not possible was described in Yessad (2006). The linear system to be solved in the spectral space in this case can be written in the following way:

$$\begin{pmatrix} \underline{\mathbf{A}}+\underline{\mathbf{C}} & \underline{\mathbf{B}} \\ \underline{\mathbf{F}} & \underline{\mathbf{E}} \end{pmatrix} \begin{pmatrix} \mathbf{D} \\ \mathbf{d} \end{pmatrix} = \begin{pmatrix} \mathbf{R}_D \\ \mathbf{R}_d \end{pmatrix}, \tag{B1}$$

where $\mathbf{R}_D$ and $\mathbf{R}_d$ describe the right-hand side of the linearized prognostic equations for D and d, respectively, and where several matrix operators have been defined as follows to simplify the notation:

$$\begin{aligned} \underline{\mathbf{A}} &= (1-\delta t^2 c^2 \Delta)\underline{\mathbf{I}}, \\ \underline{\mathbf{B}} &= \delta t^2 \Delta (RT^* \underline{\mathbf{G}} - c^2 \underline{\mathbf{I}}), \\ \underline{\mathbf{C}} &= \delta t^2 \Delta RT^* \underline{\mathbf{C}}_1, \\ \underline{\mathbf{E}} &= \underline{\mathbf{I}} - \frac{\delta t^2 c^2}{rH^2} \underline{\mathbf{L}}, \\ \underline{\mathbf{F}} &= \frac{\delta t^2}{rH^2} \underline{\mathbf{L}} (RT^* \underline{\mathbf{S}} - c^2 \underline{\mathbf{I}}). \end{aligned}$$

Here δt is the time step, $c^2 = RT^*(C_p/C_v)$ and $H = RT^*/g$ are constants, Δ is the Laplacian operator, $\underline{\mathbf{I}}$ is the identity matrix, and $\underline{\mathbf{C}}_1$ represents the constraint C1:

$$\underline{\mathbf{C}}_1 = -\underline{\mathbf{G}} \cdot \underline{\mathbf{S}} + \underline{\mathbf{G}} + \underline{\mathbf{S}} - \underline{\mathbf{N}}.$$

Then $\underline{\mathbf{C}}$ is zero for FD operators defined in Bubnová et al. (1995), and has a small but not zero spectral radius for FE operators defined here. To precondition this system, we multiply (B1) by

$$\begin{pmatrix} \underline{\mathbf{I}} & \underline{\mathbf{0}} \\ -\underline{\mathbf{F}} & \underline{\mathbf{A}} \end{pmatrix}, \tag{B2}$$

where $\underline{\mathbf{0}}$ is the all-zeros matrix. We solve the following system:

$$\begin{pmatrix} \underline{\mathbf{A}}+\underline{\mathbf{C}} & \underline{\mathbf{B}} \\ -\underline{\mathbf{F}}\cdot\underline{\mathbf{C}} & \underline{\mathbf{H}} \end{pmatrix} \begin{pmatrix} \mathbf{D} \\ \mathbf{d} \end{pmatrix} = \begin{pmatrix} \underline{\mathbf{I}} & \underline{\mathbf{0}} \\ -\underline{\mathbf{F}} & \underline{\mathbf{A}} \end{pmatrix} \begin{pmatrix} \mathbf{R}_D \\ \mathbf{R}_d \end{pmatrix}, \tag{B3}$$

where $\underline{\mathbf{H}} = \underline{\mathbf{A}} \cdot \underline{\mathbf{E}} - \underline{\mathbf{F}} \cdot \underline{\mathbf{B}}$ and $\underline{\mathbf{F}} \cdot \underline{\mathbf{A}} = \underline{\mathbf{A}} \cdot \underline{\mathbf{F}}$. The linear system (B3) is in the following form:

$$\underline{\mathbf{M}} \cdot \begin{pmatrix} \mathbf{D} \\ \mathbf{d} \end{pmatrix} = \mathbf{R}, \tag{B4}$$

where

$$\underline{\mathbf{M}} = \begin{pmatrix} \underline{\mathbf{A}}+\underline{\mathbf{C}} & \underline{\mathbf{B}} \\ -\underline{\mathbf{F}}\cdot\underline{\mathbf{C}} & \underline{\mathbf{H}} \end{pmatrix}, \tag{B5}$$

and

$$\mathbf{R} = \begin{pmatrix} \underline{\mathbf{I}} & \underline{\mathbf{0}} \\ -\underline{\mathbf{F}} & \underline{\mathbf{A}} \end{pmatrix} \begin{pmatrix} \mathbf{R}_D \\ \mathbf{R}_d \end{pmatrix}. \tag{B6}$$

To apply an iterative and efficient method for solving (B4), we split the left-hand side matrix $\underline{\mathbf{M}}$ into two terms, only the first of them containing $\underline{\mathbf{C}}$, which, as already mentioned, has a small spectral radius:

$$\underline{\mathbf{M}} = \underline{\mathbf{M}}_1 + \underline{\mathbf{M}}_2 = \begin{pmatrix} \underline{\mathbf{C}} & \underline{\mathbf{0}} \\ -\underline{\mathbf{F}}\cdot\underline{\mathbf{C}} & \underline{\mathbf{0}} \end{pmatrix} + \begin{pmatrix} \underline{\mathbf{A}} & \underline{\mathbf{B}} \\ \underline{\mathbf{0}} & \underline{\mathbf{H}} \end{pmatrix}. \tag{B7}$$

Observe that matrix $\underline{\mathbf{M}}_1$ inherits the small spectral radius from $\underline{\mathbf{C}}$, which is a property that is convenient to speed up the following iterative procedure of solving (B4):

$$\begin{aligned} \begin{pmatrix} \mathbf{D} \\ \mathbf{d} \end{pmatrix}^{(0)} &= \underline{\mathbf{M}}_2^{-1} \cdot \mathbf{R}, \\ \begin{pmatrix} \mathbf{D} \\ \mathbf{d} \end{pmatrix}^{(k+1)} &= -\underline{\mathbf{M}}_2^{-1} \cdot \underline{\mathbf{M}}_1 \cdot \begin{pmatrix} \mathbf{D} \\ \mathbf{d} \end{pmatrix}^{(k)} + \underline{\mathbf{M}}_2^{-1} \cdot \mathbf{R}. \end{aligned} \tag{B8}$$

Recently, Voitus (2017) noticed that when eliminating all variables but D, we obtain the Helmholtz equation:

$$\left(\underline{\mathbf{A}}+\underline{\mathbf{C}}-\underline{\mathbf{B}}\cdot\underline{\mathbf{E}}^{-1}\cdot\underline{\mathbf{F}}\right)\cdot\mathbf{D} = \mathbf{R}_D - \underline{\mathbf{B}}\cdot\underline{\mathbf{E}}^{-1}\cdot\mathbf{R}_d.$$

This may be solved directly even if $\underline{\mathbf{C}} \neq \underline{\mathbf{0}}$. Hence, we may get rid of the iterative procedure described here and slightly fasten the calculations.

APPENDIX C

Definition of Full-Level Positions and Layer Depths

Vertical discretization in the FD scheme is based on implicit definition of half-level hydrostatic pressures:

$$\pi_{\tilde{l}} = A_{\tilde{l}} + B_{\tilde{l}} \pi_s. \tag{C1}$$

The half-level values $A_{\tilde{l}}$ and $B_{\tilde{l}}$ are specified a priori and the values at the domain top are $A_{\tilde{0}} = B_{\tilde{0}} = 0$ and at the surface they are $A_{\tilde{L}} = 0$ and $B_{\tilde{L}} = 1$.

The FE scheme discretization is based on derivative form of (C1) (Untch and Hortal 2004):

$$\delta\pi_l = \delta A_l + \delta B_l \pi_s \tag{C2}$$

and on the following two integral conditions:

$$\underline{\mathbf{l}}_0^1 \cdot \frac{\delta \mathbf{A}}{\delta \boldsymbol{\eta}} = 0, \tag{C3}$$

$$\underline{\mathbf{l}}_0^1 \cdot \frac{\delta \mathbf{B}}{\delta \boldsymbol{\eta}} = 1, \tag{C4}$$

with all quantities being on full model levels. The depth of layer l is $\delta\eta_l = \eta_{\tilde{l}} - \eta_{\widetilde{l-1}}$ and the explicit half-level η values are defined as

$$\eta_{\bar{l}} = \frac{A_{\bar{l}}}{p_0} + B_{\bar{l}}, \tag{C5}$$

with constant reference pressure $p_0 = 101\,325$ Pa. The full-level η values are calculated as averages through

$$\eta_l = \frac{1}{2}\left(\eta_{\widetilde{l-1}} + \eta_{\bar{l}}\right). \tag{C6}$$

The differences δA_l and δB_l are defined using the conditions in (C3) and (C4). The first guess is computed from the following half-level quantities:

$$\widehat{\delta A_l} = A_{\bar{l}} - A_{\widetilde{l-1}}, \tag{C7}$$

$$\widehat{\delta B_l} = B_{\bar{l}} - B_{\widetilde{l-1}}. \tag{C8}$$

To fulfill (C4) the normalized difference δB_l is calculated as

$$\delta B_l = \frac{\widehat{\delta B_l}}{\underline{\mathbf{l}_0^1} \cdot \widehat{\frac{\boldsymbol{\delta}\mathbf{B}}{\boldsymbol{\delta\eta}}}}. \tag{C9}$$

The condition in (C3) can be rewritten into the following form:

$$\underline{\mathbf{l}_0^1} \cdot \left(\frac{1}{p_0}\frac{\boldsymbol{\delta}\mathbf{A}}{\boldsymbol{\delta\eta}} + \mathbf{J}\right) = 1 \tag{C10}$$

taking into account that $\mathbf{l}_0^1\mathbf{J} = 1$ for the all-ones vector $\mathbf{J}$.

The differences δA_l are then computed from the following relation:

$$\frac{1}{p_0}\frac{\delta A_l}{\delta\eta_l} + 1 = \frac{1}{\beta}\left(\frac{1}{p_0}\frac{\widehat{\delta A_l}}{\delta\eta_l} + 1\right), \tag{C11}$$

with constant β computed from the guess as follows:

$$\beta = \underline{\mathbf{l}_0^1} \cdot \left(\frac{1}{p_0}\widehat{\frac{\boldsymbol{\delta}\mathbf{A}}{\boldsymbol{\delta\eta}}} + \mathbf{J}\right). \tag{C12}$$

Having correct values of full-level differences from (C2) the full-level A_l and B_l are computed through

$$\underline{\mathbf{l}_0^\eta} \cdot \frac{\boldsymbol{\delta}\mathbf{A}}{\boldsymbol{\delta\eta}} = \mathbf{A}, \tag{C13}$$

$$\underline{\mathbf{l}_0^\eta} \cdot \frac{\boldsymbol{\delta}\mathbf{B}}{\boldsymbol{\delta\eta}} = \mathbf{B}. \tag{C14}$$

When using prognostic gw on half levels we need also the half-level $\widetilde{\boldsymbol{\delta}\mathbf{A}/\boldsymbol{\delta\eta}}$ and $\widetilde{\boldsymbol{\delta}\mathbf{B}/\boldsymbol{\delta\eta}}$ to evaluate $\mathbf{m}_h$ in (56). These values are computed from the spline fit of full-level values used implicitly inside $\mathbf{l}_0^\eta$ operator. We design interpolation operator omitting mass and stiffness matrices in (27) as

$$\underline{\mathbf{T}} = \underline{\mathbf{A}_h} \cdot \underline{\mathbf{A}}^{-1}, \tag{C15}$$

with $(A)_{kl} = a_k(\eta_l)$ as in (16), and $(A_h)_{k\bar{l}} = a_k(\eta_{\bar{l}})$ being projections from FE space to full model levels and to half model levels, respectively. The set of basis functions $a_k(\eta)$ and the boundary conditions are the same as used for $\underline{\mathbf{l}_0^\eta}$ in Table 1. The half-level differences of A and B yields the following:

$$\widetilde{\frac{\boldsymbol{\delta}\mathbf{A}}{\boldsymbol{\delta\eta}}} = \underline{\mathbf{T}} \cdot \frac{\boldsymbol{\delta}\mathbf{A}}{\boldsymbol{\delta\eta}}, \tag{C16}$$

$$\widetilde{\frac{\boldsymbol{\delta}\mathbf{B}}{\boldsymbol{\delta\eta}}} = \underline{\mathbf{T}} \cdot \frac{\boldsymbol{\delta}\mathbf{B}}{\boldsymbol{\delta\eta}}. \tag{C17}$$

REFERENCES

Bénard, P., 2003: Stability of semi-implicit and iterative centered-implicit time discretizations for various equation systems used in NWP. *Mon. Wea. Rev.*, **131**, 2479–2491, https://doi.org/10.1175/1520-0493(2003)131<2479:SOSAIC>2.0.CO;2.

——, 2004: On the use of a wider class of linear systems for the design of constant-coefficients semi-implicit time schemes in NWP. *Mon. Wea. Rev.*, **132**, 1319–1324, https://doi.org/10.1175/1520-0493(2004)132<1319:OTUOAW>2.0.CO;2.

——, R. Laprise, J. Vivoda, and P. Smolíková, 2004: Stability of leapfrog constant-coefficients semi-implicit schemes for the fully elastic system of Euler equations: Flat-terrain case. *Mon. Wea. Rev.*, **132**, 1306–1318, https://doi.org/10.1175/1520-0493(2004)132<1306:SOLCSS>2.0.CO;2.

——, J. Mašek, and P. Smolíková, 2005: Stability of leapfrog constant-coefficients semi-implicit schemes for the fully elastic system of Euler equations: Case with orography. *Mon. Wea. Rev.*, **133**, 1065–1075, https://doi.org/10.1175/MWR2907.1.

——, J. Vivoda, J. Mašek, P. Smolíková, K. Yessad, C. Smith, R. Brožková, and J. F. Geleyn, 2010: Dynamical kernel of the Aladin–NH spectral limited-area model: Revised formulation and sensitivity experiments. *Quart. J. Roy. Meteor. Soc.*, **136**, 155–169, https://doi.org/10.1002/qj.522.

Bubnová, R., G. Hello, P. Bénard, and J. F. Geleyn, 1995: Integration of the fully elastic equations cast in the hydrostatic pressure terrain-following coordinate in the framework of the ARPEGE/Aladin NWP system. *Mon. Wea. Rev.*, **123**, 515–535, https://doi.org/10.1175/1520-0493(1995)123<0515:IOTFEE>2.0.CO;2.

Caluwaerts, S., D. Degrauwe, P. Termonia, F. Voitus, P. Bénard, and J.-F. Geleyn, 2015: Importance of temporal symmetry in spatial discretization for geostrophic adjustment in semi-implicit Z-grid schemes. *Quart. J. Roy. Meteor. Soc.*, **141**, 128–138, https://doi.org/10.1002/qj.2344.

de Boor, C., 1978: *A Practical Guide to Splines*. Applied Mathematical Sciences Series, Vol. 27, Springer-Verlag, 348 pp., https://doi.org/10.1137/1022106.

Guerra, J. E., and P. A. Ullrich, 2016: A high-order staggered finite-element vertical discretization for non-hydrostatic atmospheric models. *Geosci. Model Dev.*, **9**, 2007–2029, https://doi.org/10.5194/gmd-9-2007-2016.

Hortal, M., 2002: The development and testing of a new two-time-level semi-Lagrangian scheme (SETTLS) in the ECMWF forecast model. *Quart. J. Roy. Meteor. Soc.*, **128**, 1671–1687, https://doi.org/10.1002/qj.200212858314.

Laprise, R., 1992: The Euler equations of motion with hydrostatic pressure as an independent variable. *Mon. Wea. Rev.*, **120**, 197–207, https://doi.org/10.1175/1520-0493(1992)120<0197:TEEOMW>2.0.CO;2.

Lorenz, E. N., 1960: Energy and numerical weather prediction. *Tellus*, **12**, 364–373, https://doi.org/10.3402/tellusa.v12i4.9420.

Lynch, D. R., 2005: *Numerical Partial Differential Equations for Environmental Scientists and Engineers: A First Practical Course.* Springer, 388 pp., https://doi.org/10.1007/b102052.

Ritchie, H., C. Temperton, A. Simmons, M. Hortal, T. Davies, D. Dent, and M. Hamrud, 1995: Implementation of the semi-Lagrangian method in a high-resolution version of the ECMWF forecast model. *Mon. Wea. Rev.*, **123**, 489–514, https://doi.org/10.1175/1520-0493(1995)123<0489:IOTSLM>2.0.CO;2.

Simarro, J., and M. Hortal, 2012: A semi-implicit non-hydrostatic dynamical kernel using finite elements in the vertical discretization. *Quart. J. Roy. Meteor. Soc.*, **138**, 826–839, https://doi.org/10.1002/qj.952.

Simmons, A. J., and D. M. Burridge, 1981: An energy and angular-momentum conserving vertical finite-difference scheme and hybrid vertical coordinates. *Mon. Wea. Rev.*, **109**, 758–766, https://doi.org/10.1175/1520-0493(1981)109<0758:AEAAMC>2.0.CO;2.

Staniforth, A., and N. Wood, 2005: Comments on "A finite-element scheme for the vertical discretization in the semi-Lagrangian version of the ECMWF forecast model" by A. Untch and M. Hortal (April B, 2004, 130, 1505–1530). *Quart. J. Roy. Meteor. Soc.*, **131**, 765–772, https://doi.org/10.1256/qj.04.10.

Straka, J. M., R. B. Wilhelmson, L. J. Wicker, J. R. Anderson, and K. K. Droegemeier, 1993: Numerical solutions of a non linear density current: A benchmark solution and comparisons. *Int. J. Numer. Methods Fluids*, **17**, 1–22, https://doi.org/10.1002/fld.1650170103.

Termonia, P., and Coauthors, 2018: The ALADIN System and its canonical model configurations AROME CY41T1 and ALARO CY40T1. *Geosci. Model Dev.*, **11**, 257–281, https://doi.org/10.5194/gmd-11-257-2018.

Untch, A., and M. Hortal, 2004: A finite-element scheme for the vertical discretization of the semi-Lagrangian version of the ECMWF forecast model. *Quart. J. Roy. Meteor. Soc.*, **130**, 1505–1530, https://doi.org/10.1256/qj.03.173.

Voitus, F., 2017: An alternative elimination procedure. Internal Note of Météo-France, Météo-France, Toulouse, France, 2 pp.

Yessad, K., 2006: Semi-implicit spectral computations in the NH version of ARPEGE/ALADIN: Specific problems when the constraint "C1" is relaxed. Météo-France Tech. Rep., Météo-France, Toulouse, France, 14 pp.